

The impact of upper tropospheric humidity from Microwave Limb Sounder on the midlatitude greenhouse effect

Hua Hu and W. Timothy Liu

Jet Propulsion Laboratory, California Institute of Technology, Pasadena, CA

Abstract. This paper presents an analysis of upper tropospheric humidity, as measured by the **Microwave Limb Sounder**, and the impact of the humidity on the **greenhouse effect** in the midlatitudes. Enhanced upper tropospheric humidity and an enhanced greenhouse effect occur over the **storm tracks** in the North Pacific and North Atlantic. In these areas, strong baroclinic activity and the large number of deep convective clouds transport more water vapor to the upper troposphere, and hence increase greenhouse trapping. The greenhouse effect increases with upper tropospheric humidity in areas with a moist upper troposphere (such as areas over storm tracks), but it is not sensitive to changes in upper tropospheric humidity in regions with a dry upper troposphere, clearly demonstrating that there are different mechanisms controlling the geographical distribution of the greenhouse effect in the midlatitudes.

1. Introduction

Despite its low measured value, upper tropospheric humidity (UTH) plays an important role in the trapping of longwave radiation emitted from the Earth and may have a strong influence on greenhouse warming. Whether UTH plays a positive or negative role in greenhouse warming is still under debate [Flohn and Kapala, 1989; Raval and Ramanathan, 1989; Lindzen, 1990; Rind, et al., 1991; Stephens and Greenwald, 1991; Inamdar and Ramanathan, 1994]; and most of these studies focused on tropical areas and very few explorations were made on extratropical regions. While water vapor integrated over the atmospheric column can be accurately derived over the ocean from the Special Sensor Microwave Imager (SSM/I) [Liu et al., 1992], measuring UTH has been difficult. Recently, preliminary measurements of UTH by the Microwave Limb Sounder (MLS) on the Upper Atmosphere Research Satellite (UARS) were made available [Read et al., 1995]. In the present study, the impact of UTH on midlatitude greenhouse warming is examined by using this set of UTH data in conjunction with other space-based measurements and model-simulated parameters. While the geographical distribution of the greenhouse effect over the tropical oceans is mainly controlled by the local sea surface temperature (SST), the cause of greenhouse warming distribution is more complicated over midlatitude oceans, as explained in this paper.

2. Upper Tropospheric Humidity

Relative humidity averaged over 200 to 500 mb has been estimated from the 6.7- μ m channel radiance measured by spaceborne sensors [Soden and Bretherton, 1993]. Soden and Fu [1995] used this relative humidity to represent UTH and found a strong correlation with the greenhouse effect over the tropical ocean but not over the midlatitude ocean. Over the tropical ocean, the variability of the air temperature is small, and the upper tropospheric relative humidity may provide a good representation of the change of UTH. Given the large changes in air temperature in the extratropics, the validity of using relative humidity to represent UTH is questionable.

The UARS MLS has taken direct measurements of water vapor content at pressure levels of 464 mb, 315 mb, 215 mb, and 146 mb since late September 1991 until the present (with some interruptions). The advantages of the MLS over other instruments are the ability to observe through cirrus-type clouds and a better vertical resolution (3 km) than that of the 6.7 μ m product [Read et al., 1995]. The best sensitivity of the MLS instrument to water vapor is at \sim 12 km height at low latitudes and \sim 7 km height at high latitudes. Therefore, we use the MLS water vapor measurements at a pressure level of 315 mb to represent the midlatitude water vapor in the upper troposphere. The data were monthly averaged to a 2.5 $^\circ$ latitude by 2.5 $^\circ$ longitude grid. Because the UARS satellite yawed 180 degrees every 36 days, the mid- and high-latitude coverages alternate between the Northern Hemisphere and the Southern Hemisphere every 36 days. Note that the MLS UTH measurements presented here are preliminary, validation and improvement of retrieval algorithm are on going research now. Nevertheless, several papers have been published based on data analysis on MLS UTH observations [e.g., Read et al., 1995; Elsen et al., 1996; Stone et al., 1996].

UTH can also be estimated by using a general circulation model. The distribution of UTH (at 300 mb) provided by the Goddard Earth Observing System - Data Assimilation System (GEOS-DAS) for July 1992 (Fig. 1a) is quite different from the distribution of UTH observed from the MLS (Fig. 2a). The UTH from the MLS has a lower magnitude and finer spatial structures aligned with the storm tracks in the North Pacific and North Atlantic; the enhanced UTH over storm tracks is superimposed on a background of latitudinal variation. The distribution of modeled UTH follows the distribution of total precipitable water obtained from the SSM/I (Fig. 1b); the precipitable water largely decreases with latitude and has less variation with longitude. Note that both the modeled UTH and total precipitable water have patterns similar to those of sea surface temperature (SST) (Fig. 1c). The discrepancies between the modeled and measured UTH may result from the lack of UTH observations available for assimilation into GEOS-DAS.

3. Other Data

The normalized greenhouse effect was calculated by using the formula $g = (\sigma T_s^4 - F) / (\sigma T_s^4)$, where T_s is the surface temperature, F is the outgoing longwave radiation (OLR) flux at the top of the atmosphere, and σ is the Stephan-Boltzmann constant [Raval and Ramanathan, 1989]. The OLR observations were ob-

tained by the nonscanner instrument in the Earth Radiation Budget Experiment (ERBE) [Luther et al., 1986]. The OLR observations from the nonscanner instrument that were used in this study include clear, cloudy, and overcast conditions because there was no scene identification information from the scanners, which were inoperative after February 1990. Due to the lack of surface temperatures obtained over land, this study focuses on the oceans, and the SST data used here were derived from Advanced Very High Resolution Radiometer (AVHRR) observations blended with in situ measurements [Reynolds and Smith, 1995]. The coverage by deep convective clouds represents a fractional area of coverage by those high clouds which have cloud top pressure less than 440 mb and optical thickness greater than 22.63. The information on deep convective clouds was provided by the International Satellite Cloud Climatology Project (ISCCP) D2 monthly mean data set [Rossow and Schiffer, 1991]. Comparison between SAGE II (Stratospheric Aerosol and Gas Experiment II) and ISCCP high-level clouds demonstrated that their geographical distributions of cloud amounts are in good agreement, both have high values in midlatitude storm tracks [Liao et al., 1995]. The ERBE and ISCCP data were obtained from the NASA Langley Research Center EOSDIS Distributed Active Archive Center. Re-analysis data produced by GEOS-DAS were used to study baroclinic activity in the midlatitudes. The monthly averages for July 1992 in the Northern Hemisphere midlatitudes (between 120° and 360°E and 30° and 55°N) were chosen for this study because the overlaps between available data sets are longer during this month.

4. The Greenhouse Effect

The enhancement in MLS UTH over storm tracks in the North Pacific and North Atlantic is collocated with an increase in the greenhouse effect, as shown in Figure 2, clearly demonstrating the ability of UTH to trap the Earth's longwave radiation. The enhancement in UTH over the storm tracks is associated with large-scale dynamical processes, such as the baroclinic waves. Figure 3a shows that deep convective cloud coverage increases over storm tracks, hence more water vapor is transported upward to the tropopause. Figure 3b indicates that the generation of these deep convective clouds is associated with synoptic-scale baroclinic waves along storm tracks (based on the analysis of GEOS-DAS model products). In this study, the baroclinic activity is measured with the baroclinicity index, namely, the maximum Eady growth rate [Lindzen and Farrell 1980]. The index was calculated by using the formula $\sigma_{BI} = 0.31 f |\partial U / \partial Z| N^{-1}$, where f is the Coriolis parameter, $\partial U / \partial Z$ is the zonal wind vertical shear, and N is the Brunt-Väisälä frequency. The data shown in Figure 3b are monthly averages of 6-hourly baroclinicity indices using wind and temperatures at 850 mb and 700 mb levels from GEOS-DAS. The higher baroclinicity index the stronger the eddy activity implied. Hoskins and Valdes (1990) showed that high baroclinicity over the winter Northern Hemisphere is located along storm track regions. Del Genio et al. [1994] used a general circulation model (GCM) to study the maintenance of upper tropospheric water vapor distribution and argued that the eddies play an impor-

tant role in moistening the extratropical upper troposphere. Baroclinic wave features were also observed in MLS upper tropospheric water vapor measurements in the extratropical Southern Hemisphere summertime [Elson et al., 1996; Stone et al., 1996]. It is worth mentioning that an increase in the amount of deep convective clouds will also enhance the greenhouse trapping (Ackerman et al., 1992). Since the greenhouse effect presented here includes observations made under clear and cloudy conditions, we do not have enough information to separate the relative contribution of upper tropospheric water vapor from that of deep convective clouds to the greenhouse effect over the storm tracks.

The impact of UTH on the greenhouse effect varies in different regions. Figure 4a shows the normalized greenhouse effect (g) plotted against UTH from the MLS (W), with the UTH values less than 0.25 g/kg , representing regions located at higher latitudes and outside storm tracks. The greenhouse effect has a low positive correlation with UTH (a correlation coefficient of $\gamma=0.26$). The greenhouse effect is also not very sensitive to the change of UTH: a straight line of $g=0.34+0.23W$ was obtained from linear least squares fits to these data, with a standard deviation of $\sigma=0.02$. However, as shown in Figure 4b, at lower latitudes and over storm tracks where UTH values are greater than 0.25 g/kg , the greenhouse effect has a stronger positive correlation with UTH (a correlation coefficient of $\gamma=0.67$). Also, the greenhouse effect is more sensitive to the change of UTH: a straight line of $g=0.15+1.0W$ was obtained from linear least squares fits to these data, with a standard deviation of $\sigma=0.02$. These results imply that at areas with higher UTH values (e.g., areas over storm tracks), large-scale dynamical processes play an important role in determining the greenhouse effect distribution. Elsewhere, the greenhouse effect is not sensitive to the change of UTH, indicating that other processes, such as local thermodynamical processes in Clausius-Clapeyron relationship, might largely control the greenhouse effect.

5. Conclusion

Although the water vapor distribution in the extratropical upper troposphere is much smaller than that in the Tropics and in the lower troposphere, the analysis of UTH data obtained from the MLS reveals the importance of water vapor in trapping the Earth's longwave radiation. It was found that the UTH from the MLS is enhanced over the storm tracks in the North Pacific and North Atlantic, collocating with an increase in the greenhouse warming. The mechanism of observed enhancement in UTH over the storm tracks seems to be associated with the increase in the amount of deep convective clouds, and thus the transportation of more water vapor upward to the tropopause. The analysis of data derived from an atmospheric general circulation model indicates that the generation of these deep convective clouds is related to synoptic-scale baroclinic waves along storm tracks. In different regions, the impact of UTH on the greenhouse effect varies: for a wetter upper troposphere, the greenhouse effect has a strong positive correlation with changes in UTH; for a drier upper troposphere, the greenhouse effect is not sensitive to a change of UTH. This suggests that greenhouse warming in different regions is controlled by different mechanisms, e.g., large-scale dynamical processes and local thermodynamical processes.

Acknowledgments. The authors thank Drs. Joe Waters and Bill Read in the Jet Propulsion Laboratory's MLS group for providing the MLS upper tropospheric water vapor data. The authors also thank the Data Assimilation Office and the Distributed Active Archive Center at the NASA Goddard Space Flight Center, for producing and distributing the data. This study was conducted at the Jet Propulsion Laboratory, California Institute of Technology, under contract with the National Aeronautics and Space Administration (NASA). This research was supported by the NASA Earth Observing System (EOS) Interdisciplinary Science Investigation.

References

- Ackerman, S. A., R. A. Frey, and W. L. Smith, Radiation budget studies using collocated observations from advanced very high resolution radiometer, high-resolution infrared sounder/2, and earth radiation budget experiment instrument, *J. Geophys. Res.*, **11**, 11,513-11,523, 1992.
- Del Genio, A. D., W. Kovari, and M.-S. Yao, Climate implications of the seasonal variation of upper tropospheric water vapor, *Geophys. Res. Lett.*, **21**, 2701-2704, 1994.
- Elson, L. S., W. G. Read, J. W. Waters, P. W. Mote, J. S. Kinnersley, and R. S. Harwood, Space-time variations in water vapor as observed by the UARS Microwave Limb Sounder, *J. Geophys. Res.*, **101**, 9001-9016, 1996.
- Flohn, H. and A. Kapala, Changes in tropical sea-air interaction processes over a thirty year period, *Nature*, **338**, 244-246, 1989.
- Hoskins, B. J., and P. J. Valdes, On the existence of storm tracks, *J. Atmos. Sci.*, **47**, 1854-1864, 1990.
- Inamdar, A. K., and V. Ramanathan, Physics of the greenhouse effect and convection in warm oceans, *J. Climate*, **7**, 715-731, 1994.
- Liao, X., W. B. Rossow, and D. Rind, Comparison between SAGE II and ISCCP high-level clouds 1. Global and zonal mean cloud amounts, *J. Geophys. Res.*, **100**, 1121-1135, 1995.
- Lindzen, R. S., and B. Farrell, A simple approximate result for the maximum growth rate of baroclinic instabilities, *J. Atmos. Sci.*, **37**, 1648-1654, 1980.
- Lindzen, R. S., Some coolness concerning global warming, *Bull. Am. Meteorol. Soc.*, **71**, 288-299, 1990.
- Liu, W. T., W. Tang and F. J. Wentz, Precipitable water and surface humidity over global ocean from Special Sensor Microwave Imager and European Center for Medium Range Weather Forecasts, *J. Geophys. Res.*, **97**, 2251-2264, 1992.
- Luther, M. R., J. E. Cooper, and G. R. Taylor, The earth radiation budget experiment nonscanner instrument, *Rev. of Geophys.*, **24**, 391-399, 1986.
- Raval, A., and V. Ramanathan, Observational determination of the greenhouse effect, *Nature*, **342**, 758-762, 1989.
- Read, W. G., J. W. Waters, D. A. Flower, L. Froidevaux, R. F. Jarnot, D. L. Hartmann, R. S. Harwood, and R. G. Rood, Upper tropospheric water vapor from UARS MLS, *Bull. Am. Meteorol. Soc.*, **76**, 2381-2389, 1995.
- Reynolds, R. W., and T. M. Smith, A high-resolution global sea surface temperature climatology, *J. Climate*, **8**, 1571-1583, 1995.
- Rind, D., E. W. Chiou, W. Chu, J. Larsen, S. Oltmans, J. Lerner, M. P. McCormick, and L. McMaster, Positive water vapor feedback in climate models confirmed by satellite data, *Nature*, **349**, 500-503, 1991.
- Rossow, W. B., and R. A. Schiffer, ISCCP cloud data product, *Bull. Amer. Meteor. Soc.*, **72**, 1-20, 1991.
- Soden, B. J., and F. P. Bretherton, Upper tropospheric relative humidity from the GOES 6.7 μ m channel: Method and climatology for July 1987, *J. Geophys. Res.*, **98**, 16,669-16,688, 1993.
- Soden, B. J., and R. Fu, A satellite analysis of deep convection, upper-tropospheric humidity, and the greenhouse effect, *J. Climate*, **8**, 2335-2351, 1995.
- Stephens, G. L., and T. J. Greenwald, The earth's radiation budget and its relation to atmospheric hydrology. 1. Observations of the clear sky greenhouse effect, *J. Geophys. Res.*, **96**, 15311-15324, 1991.
- Stone, E. M., W. J. Randel, J. L. Stanford, W. G. Read, J. W. Waters, Baroclinic wave variations observed in MLS upper tropospheric water vapor, *Geophys. Res. Lett.*, **23**, 2967-2970, 1996.

(Received March 5, 1998; revised June 3, 1998;
accepted June 24, 1998.)

Figure 1. (a) Modeled upper tropospheric specific humidity at 300 mb from GEOS-DAS. The contour interval is 0.1 g/kg; values greater than 0.3 g/kg and 0.4 g/kg are denoted by light and dark shading, respectively. (b) Total precipitable water data from the SSM/I. The contour interval is 0.3 g/cm²; values greater than 2.3 g/cm² and 2.9 g/cm² are denoted by light and dark shading, respectively. (c) Sea surface temperature from the AVHRR. The contour level is 5°C; values greater than 15°C and 20°C are denoted by light and dark shading, respectively. The data for 1(a) through 1(c) are monthly averages for July 1992.

Figure 2. (a) Upper tropospheric specific humidity from the MLS at 315 mb. The contour interval is 0.03 g/kg; values greater than 0.24 g/kg and 0.27 g/kg are denoted by light and dark shading, respectively. (b) The normalized greenhouse effect. The contour interval is 0.02; values greater than 0.4 and 0.42 are denoted by light and dark shading, respectively. The data in 2(a) and 2(b) are monthly averages for July 1992.

Figure 3. (a) Deep convective cloud amount from the ISCCP D2 monthly averages for July 1992. The contour interval is 2%; values greater than 2% and 4% are denoted by light and dark shading, respectively. (b) Calculated monthly averages of 6-hourly baroclinicity indices using GEOS-DAS re-analysis data. The contour interval is 0.04 day⁻¹; values larger than 0.2 day⁻¹ and 0.24 day⁻¹ are denoted by light and dark shading, respectively.

Figure 4. (a) The normalized greenhouse effect plotted against upper tropospheric specific humidity (UTH) from the MLS with the UTH values less than 0.25 g/kg; the straight line is a fit to these data. (b) the same comparison and parameters as in Figure 4(a) as except with the UTH values greater than 0.25 g/kg.

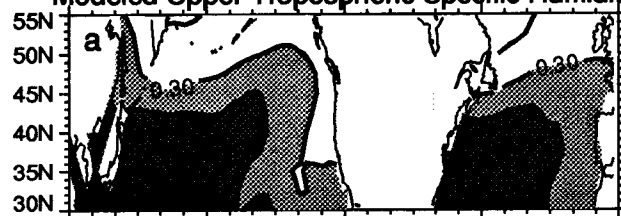
Figure 1. (a) Modeled upper tropospheric specific humidity at 300 mb from GEOS-DAS. The contour interval is 0.1 g/kg; values greater than 0.3 g/kg and 0.4 g/kg are denoted by light and dark shading, respectively. (b) Total precipitable water data from the SSM/I. The contour interval is 0.3 g/cm²; values greater than 2.3 g/cm² and 2.9 g/cm² are denoted by light and dark shading, respectively. (c) Sea surface temperature from the AVHRR. The contour level is 5°C; values greater than 15°C and 20°C are denoted by light and dark shading, respectively. The data for 1(a) through 1(c) are monthly averages for July 1992.

Figure 2. (a) Upper tropospheric specific humidity from the MLS at 315 mb. The contour interval is 0.03 g/kg; values greater than 0.24 g/kg and 0.27 g/kg are denoted by light and dark shading, respectively. (b) The normalized greenhouse effect. The contour interval is 0.02; values greater than 0.4 and 0.42 are denoted by light and dark shading, respectively. The data in 2(a) and 2(b) are monthly averages for July 1992.

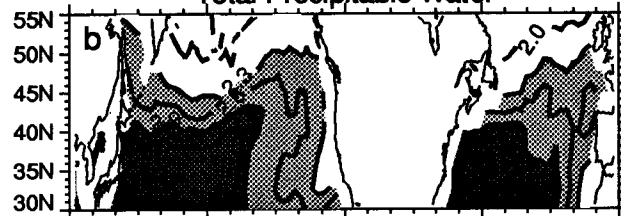
Figure 3. (a) Deep convective cloud amount from the ISCCP D2 monthly averages for July 1992. The contour interval is 2%; values greater than 2% and 4% are denoted by light and dark shading, respectively. (b) Calculated monthly averages of 6-hourly baroclinicity indices using GEOS-DAS re-analysis data. The contour interval is 0.04 day⁻¹; values larger than 0.2 day⁻¹ and 0.24 day⁻¹ are denoted by light and dark shading, respectively.

Figure 4. (a) The normalized greenhouse effect plotted against upper tropospheric specific humidity (UTH) from the MLS with the UTH values less than 0.25 g/kg; the straight line is a fit to these data. (b) the same comparison and parameters as in Figure 4(a) as except with the UTH values greater than 0.25 g/kg.

Modeled Upper Tropospheric Specific Humidity



Total Precipitable Water



Sea Surface Temperature

